

UC Irvine

UC Irvine Previously Published Works

Title

Role of PDZK1 Protein in Apical Membrane Expression of Renal Sodium-coupled Phosphate Transporters*

Permalink

<https://escholarship.org/uc/item/7d0742xv>

Journal

Journal of Biological Chemistry, 286(17)

ISSN

0021-9258

Authors

Giral, Hector
Lanzano, Luca
Caldas, Yupanqui
[et al.](#)

Publication Date

2011-04-01

DOI

10.1074/jbc.m110.199752

Supplemental Material

<https://escholarship.org/uc/item/7d0742xv#supplemental>

Copyright Information

This work is made available under the terms of a Creative Commons Attribution License, available at <https://creativecommons.org/licenses/by/4.0/>

Peer reviewed

Role of PDZK1 Protein in Apical Membrane Expression of Renal Sodium-coupled Phosphate Transporters*[§]

Received for publication, November 2, 2010, and in revised form, February 17, 2011. Published, JBC Papers in Press, March 9, 2011, DOI 10.1074/jbc.M110.199752

Hector Giral^{†1}, Luca Lanzano^{§1}, Yupanqui Caldas[‡], Judith Blaine[‡], Jill W. Verlander[¶], Tim Lei^{||}, Enrico Gratton[§], and Moshe Levi^{†2}

From the [†]Department of Medicine, University of Colorado, Aurora, Colorado 80045, the [§]Laboratory for Fluorescence Dynamics, University of California, Irvine, California 92697, the [¶]Department of Medicine, Division of Nephrology, Hypertension, and Transplantation, University of Florida, Gainesville, Florida 32610, and the ^{||}Department of Electrical Engineering, University of Colorado Denver, Denver, Colorado 80202

The sodium-dependent phosphate (Na/P_i) transporters NaPi-2a and NaPi-2c play a major role in the renal reabsorption of P_i. The functional need for several transporters accomplishing the same role is still not clear. However, the fact that these transporters show differential regulation under dietary and hormonal stimuli suggests different roles in P_i reabsorption. The pathways controlling this differential regulation are still unknown, but one of the candidates involved is the NHERF family of scaffolding PDZ proteins. We propose that differences in the molecular interaction with PDZ proteins are related with the differential adaptation of Na/P_i transporters. *Pdzk1*^{-/-} mice adapted to chronic low P_i diets showed an increased expression of NaPi-2a protein in the apical membrane of proximal tubules but impaired up-regulation of NaPi-2c. These results suggest an important role for PDZK1 in the stabilization of NaPi-2c in the apical membrane. We studied the specific protein-protein interactions of Na/P_i transporters with NHERF-1 and PDZK1 by FRET. FRET measurements showed a much stronger interaction of NHERF-1 with NaPi-2a than with NaPi-2c. However, both Na/P_i transporters showed similar FRET efficiencies with PDZK1. Interestingly, in cells adapted to low P_i concentrations, there were increases in NaPi-2c/PDZK1 and NaPi-2a/NHERF-1 interactions. The differential affinity of the Na/P_i transporters for NHERF-1 and PDZK1 proteins could partially explain their differential regulation and/or stability in the apical membrane. In this regard, direct interaction between NaPi-2c and PDZK1 seems to play an important role in the physiological regulation of NaPi-2c.

control phosphate homeostasis. NaPi-2a (NaPiIIa) is responsible for ~70% of the P_i reabsorbed in the adult kidney of mice, whereas NaPi-2c (NaPiIIc) handles the remaining 30% (1, 2). A low dietary P_i intake induces an increase of P_i reabsorption in the proximal tubule mediated by augmented apical expression of NaPi-2a and NaPi-2c transporters and consequent increased P_i uptake (3–6).

Despite sharing a very similar molecular structure, NaPi-2a and NaPi-2c exhibit an increasing list of physiological differences. For example, whereas NaPi-2a is electrogenic, NaPi-2c is electroneutral (4, 7). In addition, both transporters participate in the renal adaptation to changes in dietary P_i with different characteristics. In response to a high P_i intake, NaPi-2a abundance decreases quickly (less than 1 h), internalization takes place in a microtubule-independent way, and molecules are targeted to the lysosomes via endosomes (8, 9). In contrast, under a high P_i intake, NaPi-2c abundance decreases slowly (4 h), molecules are internalized through a microtubule-dependent pathway, and rather than being degraded, they are accumulated in a subapical compartment (10). Similar differences have been also reported for the response of NaPi-2a and NaPi-2c to PTH (11).

Some of these differences may be explained by the type and number of proteins with which the transporters interact. For example, it is well known that NaPi-2a is integrated in a series of macromolecular complexes whose architecture is based on PDZ (PSD-95, discs-large, and ZO-1) protein interactions (12–19). NaPi-2a participates in this complex by means of a class I PDZ-binding site located at its C terminus, comprising its last three amino acids (TRL).

Using two-hybrid systems and co-immunoprecipitation, it has been previously determined that NaPi-2c interacts with the PDZ protein sodium-hydrogen exchange-regulating factor 1 (NHERF-1) and 3 (NHERF-3 or PDZK1) (15). These interactions were surprising because NaPi-2c does not have a prototypical PDZ binding motif in the C terminus (QQQL). NaPi-2c/PDZK1 interaction was stronger than NaPi-2c/NHERF-1 interaction by two-hybrid system assays, but co-immunoprecipitation was more robust for NHERF-1 than for PDZK1. Moreover, it was proposed that NaPi-2c interaction was mediated through the C-terminal end of the transporter for PDZK1 but not for NHERF-1. NaPi-2c mutants missing the C terminus were still able to interact with NHERF-1, so an unknown internal motif of NaPi-2c was proposed to interact with the first PDZ

The type II sodium-coupled phosphate (Na/P_i)³ transporters are the molecules responsible for tubular reabsorption of P_i and are the target of hormonal and nonhormonal mechanisms that

* This work was supported, in whole or in part, by National Institutes of Health Grants R01 DK066029 (M. L., Y. C., L. L., H. G., and E. G.), P41-RR03155 (to E. G. and L. L.), P50-GM076516 (to E. G. and L. L.), and K08 DK080989 (to J. B.).

[§] The on-line version of this article (available at <http://www.jbc.org>) contains supplemental Figs. S1–S8.

¹ Both authors contributed equally to this work.

² To whom correspondence should be addressed: University of Colorado Denver, 12700 East 19th Ave., Research 2, Rm. 7002, Aurora, CO 80045. Tel.: 303-724-4825; Fax: 303-724-4868; E-mail: Moshe.Levi@ucdenver.edu.

³ The abbreviations used are: Na/P_i, sodium-dependent phosphate; NHERF, sodium-hydrogen exchange-regulating factor; BBM, brush border membrane; PTH, parathyroid hormone; OK, opossum kidney; FLIM, fluorescence lifetime imaging; Cer, Cerulean.

motif of NHERF-1. Both confocal and total internal reflection microscopy showed that NaPi-2c colocalized with PDZK1 and NHERF-1 in the apical microvilli.

The depletion of PDZK1 expression in the knock-out mouse model (*Pdzk1*^{-/-} mice) does not induce major changes in the expression and regulation of NaPi-2a in the proximal tubule in response to acute or chronic alterations in dietary P_i (20). However, there was a slight reduction in NaPi-2a apical membrane protein expression when mice were fed a high phosphate diet, presumably inducing a higher phosphate excretion rate in this condition.

The functional significance of the NaPi-2c and PDZK1 interactions, however, remains unknown. The purpose of the present study was to determine whether the absence of PDZK1 modulates NaPi-2c trafficking and apical membrane expression and also to determine whether these effects are specific for the NaPi-2c transporter. In an attempt to determine the role of PDZ proteins in the differential regulation of the Na/P_i transporters, we studied the *Pdzk1*^{-/-} mouse model under chronic dietary P_i conditions.

EXPERIMENTAL PROCEDURES

Animal Procedures—The experiments were performed in *Pdzk1*^{-/-} (PDZK1/NHERF-3 KO), and corresponding age and sex-matched wild type control mice were obtained from Jackson Laboratories (Bar Harbor, ME). This knock-out animal was generated by the laboratory of David Silver (21) in a way similar to the KO described before by Kocher *et al.* (22). Expression of PDZK1 protein was tested by Western blot (with a polyclonal rabbit anti-PDZK1 kindly provided by David Silver), confirming complete abolition in the *Pdzk1*^{-/-} (supplemental Fig. S1). The animals were maintained on a 12-h light/12-h dark cycle. The mice were acclimated on regular chow diet, and they were then fed *ad libitum* a high P_i (1.5% Pi) or a low P_i (0.1% Pi) diet (Harlan Teklad, Wisconsin) for 7 days. We studied 24 mice for each experimental group including female and male animals for biochemical studies in three independent experiments. For *in vivo* perfusion fixation, we used *n* = 10 mice for immunohistochemistry and immunofluorescence microscopy studies, all of them fed a low P_i diet. The animal studies were approved by the Animal Care and Use Committee at the University of Colorado Denver.

Brush Border Membrane (BBM) Isolation—The mice were anesthetized via an intraperitoneal injection of 50 mg/kg pentobarbital sodium (Pentothal; Abbott Laboratories). After clamping of the renal vessels, blood was drawn for biochemical analysis, and the kidneys were removed for BBM isolation.

Kidney slices from two mice were combined in 7.5 ml of isolation buffer consisting of 15 mM Tris·HCl, pH 7.4, 300 mM mannitol, 5 mM EGTA, and one Roche Complete inhibitor tablet/250 ml of buffer. The kidney slices were homogenized using a Potter-Elvehjem homogenizer with 8–10 rapid strokes. An aliquot of the total homogenate fraction was taken apart for further analysis. BBM was prepared by a double Mg²⁺ precipitation. For the first Mg²⁺ precipitation, MgCl₂ was added to the homogenate (final concentration, 15 mM), and the solution was shaken every 5 min on ice for 20 min before centrifugation at 2,500 × *g* for 15 min. The pellet obtained in this step was resus-

ended and stored for analysis as Non-BBM fraction. This fraction shows enrichment in all the other cellular membranes apart from the apical plasma membrane, including Golgi apparatus, endosomes, and other trafficking compartments. The supernatant was subjected to a second Mg²⁺ precipitation, and from the resulting supernatant, the BBM was recovered by centrifugation at 38,000 × *g* for 40 min.

Western Blot Analysis—BBM proteins (20 or 30 μg), total membranes (60 μg), and non-BBM (40 μg) fractions were separated in 7.5% SDS-PAGE gels and transferred onto nitrocellulose membranes. The membranes were blocked with 5% milk in PBS with 0.1% Tween 20 (PBST) before incubation with primary antibodies overnight at 4 °C. Polyclonal rabbit anti-NaPi-2a (23) and polyclonal rabbit anti-NaPi-2c produced by Davids Biotechnology were used at 1:5000 dilution. The specificity of the anti-NaPi-2c antibody was tested by blocking peptide assay (supplemental Fig. S2). Commercial mouse monoclonal antibody AC-15 was used at 1:10,000 dilution (Sigma). After three washes with PBST, the membranes were incubated with HRP-linked secondary antibodies diluted 1:5,000 for 1 h followed for several washes with PBST. The membranes were incubated with SuperSignal West Pico Chemiluminescent Substrate (Pierce) following the manufacturer's instructions. The images were acquired and analyzed by densitometry using a Biospectrum 500 imaging system (UVP).

RNA Isolation and Real Time Quantitative PCR—Total RNA was isolated after homogenization of kidney slices using the Qiagen RNeasy mini kit. cDNA was synthesized using iScript cDNA Synthesis (Bio-Rad), and the mRNA level was quantified using a Bio-Rad iCycler real time PCR machine. NaPi-2a- and NaPi-2c-specific primers were used to quantify the Na/P_i transporters as described before (23). Cyclophilin A was used as an internal control, and the amount of RNA was calculated by the comparative threshold cycle method as recommended by the manufacturer. All of the data were calculated from duplicate reactions.

Immunofluorescence Microscopy—Mice anesthetized with isoflurane inhalent were perfused *in vivo* with PBS for 30 s followed by 2% paraformaldehyde-lysine-periodate for 8 min through cardiac puncture under controlled pressure conditions. Kidney samples were immersed in paraformaldehyde-lysine-periodate at 4 °C for 2 h and then rinsed with serial dilutions of sucrose (5, 10, and 25%) solutions. Kidney slices were embedded in optimum cutting temperature solution and frozen in liquid nitrogen. Sections 5 μm thick were cut on a Leica cryostat and stored at -20 °C until ready to use. The sections were blocked for 30 min with PBS containing 0.1% Triton X-100 and 10% goat serum. Primary antibodies were incubated with the same solution overnight at 4 °C. Polyclonal rabbit anti-NaPi-2a and anti-NaPi-2c were used at 1:500 and 1:100, respectively. The specificity of the signal obtained with anti-NaPi-2c was tested by peptide blocking assay (supplemental Fig. S2). After three washes with PBS-Triton X-100, secondary antibody Alexa-Fluor 568 was incubated for 1 h together with phalloidin-Alexa 488 to stain actin filaments. Imaging was performed on a Zeiss 510 LSM laser scanning confocal microscope (Carl Zeiss Microimaging, Thornwood, NY).

PDZK1 Regulation of NaPi-2c Transporter

Immunohistochemistry—Slices of kidney, perfusion-fixed as described above, were immersed in paraformaldehyde-lysine-periodate at 4 °C overnight, then rinsed in PBS, dehydrated in a graded series of ethanols, and infiltrated and embedded in polyester wax (polyethylene glycol 400 distearate (Polysciences, Warrington, PA), 10% cetyl alcohol).

Sections 3 μm thick were dewaxed in a graded series of ethanols, rinsed in PBS, and incubated in Trilogy antigen retrieval solution (Cell Marque, Sacramento, CA) for 1 h at 95 °C. The sections were washed in PBS, treated with 3% H_2O_2 and then 5% normal goat serum in PBS, and incubated with the anti-NaPi-2c primary antibody diluted 1:2000 or 1:4000 or the NaPi-2a primary antibody diluted 1:4000 in PBS overnight at 4 °C. The samples were washed, exposed to anti-rabbit polymer-linked peroxidase-conjugated secondary antibody (MACH2 rabbit, Biocare Medical, Concord, CA), washed, reacted with diaminobenzidine (Vector Laboratories, Burlingame, CA) for 5 min, washed in distilled water, dehydrated in graded ethanols followed by xylene, and mounted on glass slides with Eukitt mounting medium (Hawthorne, NY). The sections were photographed using a Nikon LaboPhot-2 microscope equipped with a Nikon DS-5 M digital color camera and NIS Elements software (Nikon USA, Melville, NY).

Plasma and Urine Analysis—Blood samples were collected in heparin containing tubes during sacrifice. Spot urine was collected in animals adapted to P_i diets for 1 week. Plasma obtained after centrifugation and urine samples were analyzed for P_i concentrations by using the commercial kit Stanbio Liqui-UV (Stanbio, Boerne, TX). Creatinine concentration in urine was determined using A QuantiChrom creatinine assay (BioAssay Systems, Hayward, CA). FGF-23 (C-terminal) and intact PTH were determined with specific ELISA kits from Immunotopics (San Clemente, CA). Eight or nine animals/group were used in these assays.

Cell Culture and Transfection—Opossum kidney (OK) cells (OKP clone (24)) were grown in DMEM/F-12 supplemented with 10% fetal bovine serum, penicillin, streptomycin, and L-glutamine in 37 °C CO_2 controlled 95% humidified incubator, as reported (25, 26). Transfections were achieved with Lipofectamine 2000 (Invitrogen) and cells at 90% confluency, following the manufacturer's instructions. OK cells expressing the fluorescent fusion proteins were grown on poly-L-lysine-coated eight-well Lab-Tek chambered coverglass (Nunc). To test the chronic adaptive response of OK cells to varying P_i content in the medium, transfected cells were incubated for 24 h before the measurement in a medium containing a concentration of 1 mM P_i (normal), 0.1 mM P_i (low), and 2 mM P_i (high), respectively. The measurements were performed 24–48 h after transfection.

Microscope Setup—A Zeiss LSM 510 confocal microscope (Jena, Germany), equipped with a Confocor 3 unit and the META detector was used for the images. Fluorescence lifetime imaging (FLIM) was performed using a FLIMBox imaging system coupled to the microscope. The FLIMBox is a digital frequency domain setup capable of multi-harmonic analysis whose details can be found elsewhere (27). A diode laser pulsed at a repetition rate of 20 MHz was used for the excitation at 445 nm of the Cerulean (Cer) constructs with minimal YFP cross-

excitation. Emission intensity from Cerulean was collected in the spectral window 470–495 nm. A solution of fluorescein at PH9 was used as a reference standard to calibrate the instrumental response.

Images were obtained in the 256×256 format (size variable in the range 15–25 μm depending on the cell), with a pixel dwell time of 12.5 μs and averaging over 20 frames. Fluorescent intensity was monitored during the acquisition to avoid artifacts because of photobleaching (27). FLIMBox images containing lifetime and intensity information were acquired using SimFCS software, whereas standard intensity images were saved in the LSM format through the Zeiss LSM 510 software.

Processing of FLIM-FRET Data—All of the FLIM images were analyzed in SimFCS using the so-called phasor approach (28–31), aimed to quantify FRET through the measurement of the lifetime of the donor (32, 33). The phasor represents the fluorescence decay in a Fourier transformed space. In our digital frequency domain approach, the modulation and phase measured at each pixel of an image are used directly to determine the coordinates of the phasor in this two-dimensional space. In this experiment, we analyzed the second harmonic component of the data, which corresponds to a frequency of 40 MHz. In frequency modulation technique, the optimal frequency for measuring a lifetime τ is given approximately by $1/2\pi\tau$ (28). If we take into account the range of lifetimes measured in our experiments ($\tau \sim 3$ ns for Cerulean (34) and $\tau \sim 4$ ns for the fluorescein standard), the frequency of the second harmonic is closer to the optimal value.

The phasor associated to a cell imaged with FLIM was determined as the average phasor of the pixels corresponding to the cell image. The phasor of the autofluorescence was determined by imaging nontransfected cells. The autofluorescence signal was always less than 0.5% of the signal coming from transfected cells. The phasor of the unquenched donor was determined by imaging cells transfected only with Cer-NaPi-2a (for the interaction of NaPi-2a with NHERF-1 and PDZK-1) or Cer-NaPi-2c (for the interaction of NaPi-2c with NHERF-1 and PDZK-1). For each experiment, we collected multiple images of single cells (from four to seven images) focusing at the level of the apical membrane. For each cell, we extracted the coordinates of the corresponding average phasor. The average of the phasors of all the cells was assigned to the average position of the unquenched donor (D_{unq}). The same protocol was used to measure the phasor of cells co-transfected with both donor (Cer-NaPi-2a or Cer-NaPi-2c) and acceptor species (EYFP-NHERF-1 or EYFP-PDZK1) and incubated in media with different P_i content.

FRET Analysis in the Phasor Plot—The quantification of FRET in the phasor plot is achieved by analyzing the phasor shift occurring between the two species of the donor and donor in the presence of the acceptor. Following the method described in Ref. 30, the phasors of the autofluorescence (*af*) and of the unquenched donor (D_{unq}) have been determined in each experiment so that a trajectory of variable efficiency (0–100%) could be calculated (see supplemental Fig. S5). A point along this trajectory corresponds to a pure species of donor quenched (D_q) with FRET efficiency *E*.

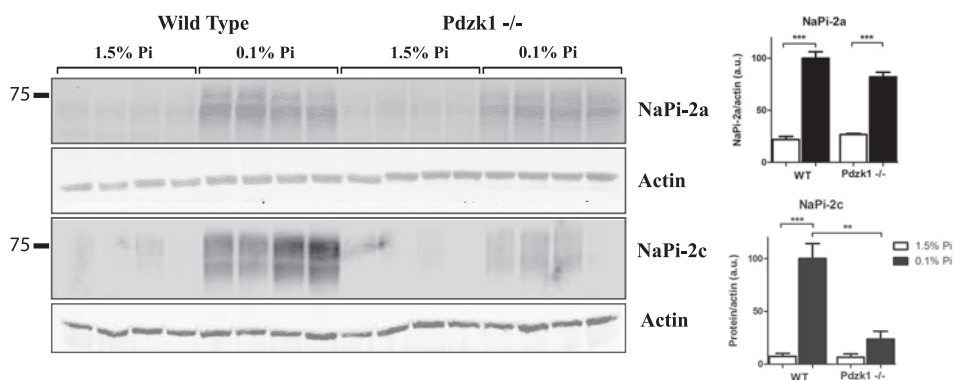


FIGURE 1. Brush Border Membrane Vesicles protein expression in WT and *Pdzk1*^{-/-} female mice in response to chronic adaptation to high (1.5%) and low (0.1%) P_i diets. NaPi-2a protein expression in BBM in *Pdzk1*^{-/-} mice adapt normally to low P_i diets in a similar way as wild type animals. However, NaPi-2c shows impaired up-regulation to low P_i diet in *Pdzk1*^{-/-} model.

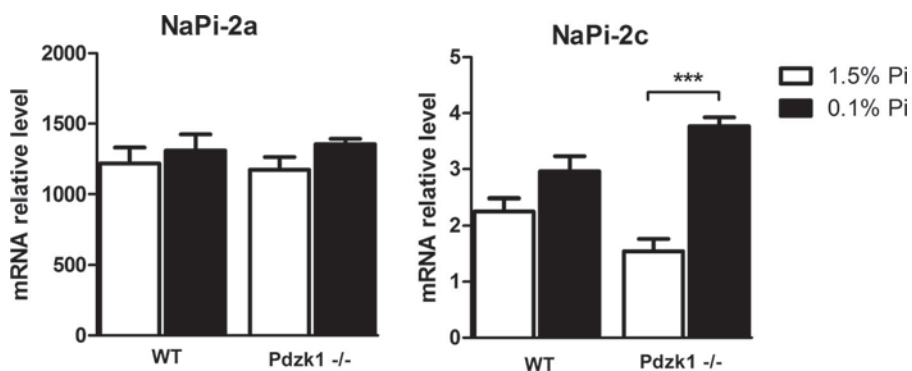


FIGURE 2. mRNA expression of NaPi-2a and NaPi-2c. Kidney mRNA samples of wild type and *Pdzk1*^{-/-} animals fed high and low P_i diets chronically were analyzed. Expression of NaPi-2a mRNA was unaffected in the *Pdzk1*^{-/-} mice, whereas NaPi-2c mRNA expression undergoes a significant increase under low P_i diet treatments.

More generally, and especially in the case of intermolecular FRET (35), a pixel may contain a mixture of quenched and unquenched donors with fractions f_q and f_{unq} , respectively. In this case, the phasor is a normalized linear combination of the phasors of D_q and D_{unq} ($f_{unq}D_{unq} + f_qD_q$) and is located along the segment connecting them, at a distance from D_{unq} proportional to the fraction of interacting donors, f_q (supplemental Fig. S5).

The efficiency trajectory was calculated for each experiment based on the average position of the donor only (D_{unq}) and the autofluorescence in the phasor plot. As a matter of fact, the experimental positions of the phasors of the donor-acceptor samples did not lie along the efficiency trajectory. Indeed they were better described by a linear combination of quenched and unquenched donor species. The quenched donor (D_q) position has been determined as the intersection between a linear fit of the data and the efficiency trajectory, in a way analogous to that described in Ref. 31 for a mixture of single exponential components. The position of D_q yields the value of efficiency E associated with the FRET interaction. The fraction of interacting donors (f_q) was then calculated directly from the position of the data points along the line connecting D_{unq} and D_q (supplemental Fig. S6).

Statistical Analysis—The results are presented as the means \pm S.E. for at least three independent experiments. The data were analyzed by analysis of variance and Student-Newman-Keul's tests for multiple comparisons or by Student's t test for unpaired data between two groups. Statistical significance

was accepted at the $p < 0.05$ level. The symbols used in the graphs are *ns* for not significant, * for $p < 0.05$, ** for $p < 0.01$, and *** for $p < 0.001$.

RESULTS

NaPi-2c Adaptation to a Low P_i Diet Is Impaired in PDZK1 Knock-out Mice—Renal Brush Border Membrane Vesicles were isolated from wild type and *Pdzk1*^{-/-} mice adapted to chronic low (0.1%) and high (1.5%) P_i diets. Western blot analysis showed that apical brush border membrane protein expression of NaPi-2a was up-regulated under low P_i diets both in wild type and *Pdzk1*^{-/-} mice (Fig. 1). *Pdzk1*^{-/-} mice demonstrated a significantly impaired up-regulation of NaPi-2c protein levels compared with the wild type animal under the same conditions (Fig. 1).

Because we initially performed this study in female animals—because of availability in our colony—we wanted to be sure that the described effects were not sex-dependent. We therefore repeated the same experiments in male wild type control and *Pdzk1*^{-/-} mice. The same impaired up-regulation of NaPi-2c occurred in male *Pdzk1*^{-/-} animals when compared with wild type animals fed low P_i diets, whereas NaPi-2a up-regulation was intact and normal (supplemental Fig. S3). These results suggested a differential involvement of PDZK1 in the adaptation of NaPi-2a versus NaPi-2c to low P_i diet.

There were no significant differences and notably no increases in NaPi-2a or NaPi-2c mRNA abundance in adapta-

PDZK1 Regulation of NaPi-2c Transporter

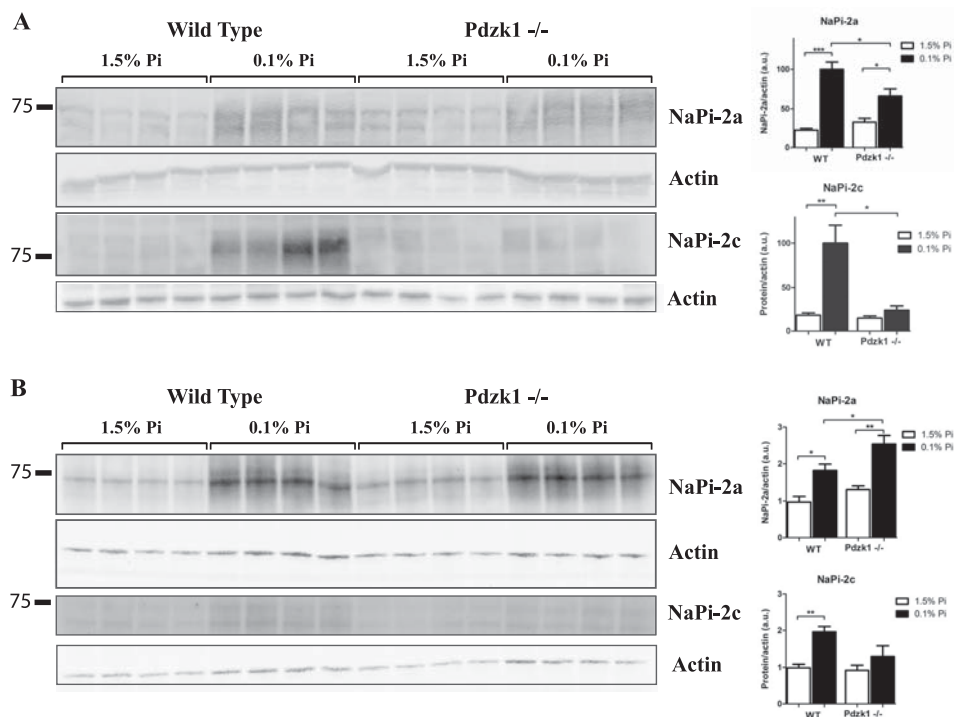


FIGURE 3. NaPi-2c protein expression is impaired in total homogenates and non-BBM fractions. Total homogenates fractions corresponding to the first homogenate of the kidneys (A) and non-BBM fractions corresponding to the pellet obtained after the first Mg precipitation in the isolation of BBM from wild type and *Pdzk1*^{-/-} animals (B) were analyzed by Western blot. NaPi-2a expression is clearly up-regulated in both animal groups under low P_i dietary conditions. However, regulation of NaPi-2c expression is impaired also at the level of total cellular protein in a similar way as shown in the apical membranes.

tion to low P_i diets in the wild type mice (Fig. 2). Nevertheless, the impaired regulation of NaPi-2c in the PDZK1 KO seems to be independent of transcription because NaPi-2c mRNA expression was significantly increased in the low P_i condition in the *Pdzk1*^{-/-} animals. We consider that increased mRNA expression is a compensatory mechanism triggered by the reduced apical expression of the transporter. Exclusion of transcriptional regulation as a mechanism for the impaired regulation of NaPi-2c suggests that post-translational mechanisms are involved.

To study how the depletion of PDZK1 was affecting the expression of NaPi-2c in the BBM, we tested the expression of NaPi-2c protein in homogenates. Total membrane renal homogenates, prepared as described under “Experimental Procedures,” were analyzed by Western blot. In wild type animals fed low P_i diets, both NaPi-2a and NaPi-2c undergo an increase in the total protein expression (Fig. 3A). *Pdzk1*^{-/-} mice are able to adapt properly in the case of NaPi-2a but show a significantly deficient up-regulation of NaPi-2c.

We also used the first Mg precipitation fraction of the BBM isolation or non-BBM fraction to test the expression of the Na/P_i transporters. There were no major differences in NaPi-2a expression between WT and *Pdzk1*^{-/-} mice, although a significant increase was observed in the KO mice under low P_i diet when compared with the wild type mice. NaPi-2c expression was clearly reduced also in this fraction in the KO animals adapted to low P_i diets (Fig. 3B).

In mice fed a low P_i diet, immunofluorescence and immunohistochemistry studies demonstrated significant differences in the effect of PDZK1 knock-out on the localization of NaPi-2c

protein. NaPi-2a immunolabel was present in proximal tubules throughout the renal cortex, primarily in the brush border, and there were no differences between WT and *Pdzk1*^{-/-} mice (data not shown). Immunostaining was more intense in convoluted proximal tubules in the cortical labyrinth than in straight proximal tubules in the medullary rays. These results were in accordance with the previous study by Capuano *et al.* (20).

In contrast, the distribution of NaPi-2c immunoreactivity was strongly affected by PDZK1 deletion. In WT mice, NaPi-2c immunolabel was present in the brush border in numerous proximal tubules throughout the cortex and was particularly intense in a small population of proximal tubule profiles near the corticomedullary junction (Figs. 4B and 5C). Brush border label was clearly evident in initial proximal tubule segments, identified by continuity with Bowman’s capsule (Fig. 5B). Straight proximal tubules in the cortex and in the outer stripe of the outer medulla generally did not exhibit brush border NaPi-2c immunolabel. In *Pdzk1*^{-/-} mice, the brush border NaPi-2c immunolabel was virtually abolished in the cortical proximal tubule profiles (Figs. 4C and 5, D and E), with the exception of a small population of proximal tubule profiles near the corticomedullary junction that retained intense brush border immunolabel (Figs. 4D and 5F). However, even these few tubules seem to have reduced expression compared with the WT mice. Moreover, a punctate intracellular staining was present in proximal tubules throughout the cortex and outer stripe of the outer medulla (Figs. 4 and 5 and supplemental Fig. S4). Thus, PDZK1 knock-out eliminated brush border NaPi-2c localization from virtually all proximal tubule profiles and enhanced NaPi-2c localization in intracellular sites. The major-

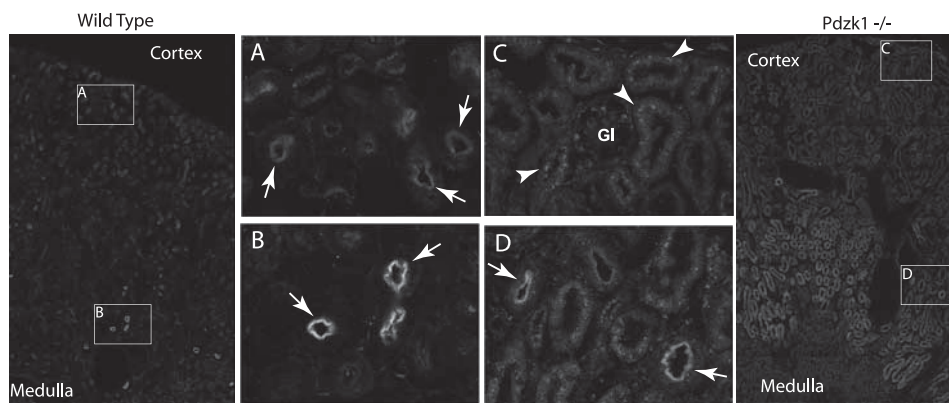


FIGURE 4. NaPi-2c localization by immunofluorescence showed differential staining pattern in wild type and *Pdzk1*^{-/-} mice. General views of kidney sections showing the cortex, corticomedullary junction, and medulla are shown for wild type (far left panel) and *Pdzk1*^{-/-} (far right panel). The zoomed views show clear differences in the cortical staining (A and C) where the apical staining (arrows) in the wild type is diminished in the KO mice that had brighter intracellular staining (arrowheads). Corticomedullary regions showed a more intense apical staining than cortex in wild type mice (B) that was not completely diminished in *Pdzk1*^{-/-} but was significantly reduced (D). Again, an intracellular staining pattern was more obvious in the KO mice samples. Interestingly, this intense intracellular staining was continued in the outer stripe of the outer medulla. *Gl*, glomeruli. Images of single tubules showing the described staining patterns are included in supplemental Fig. S4.

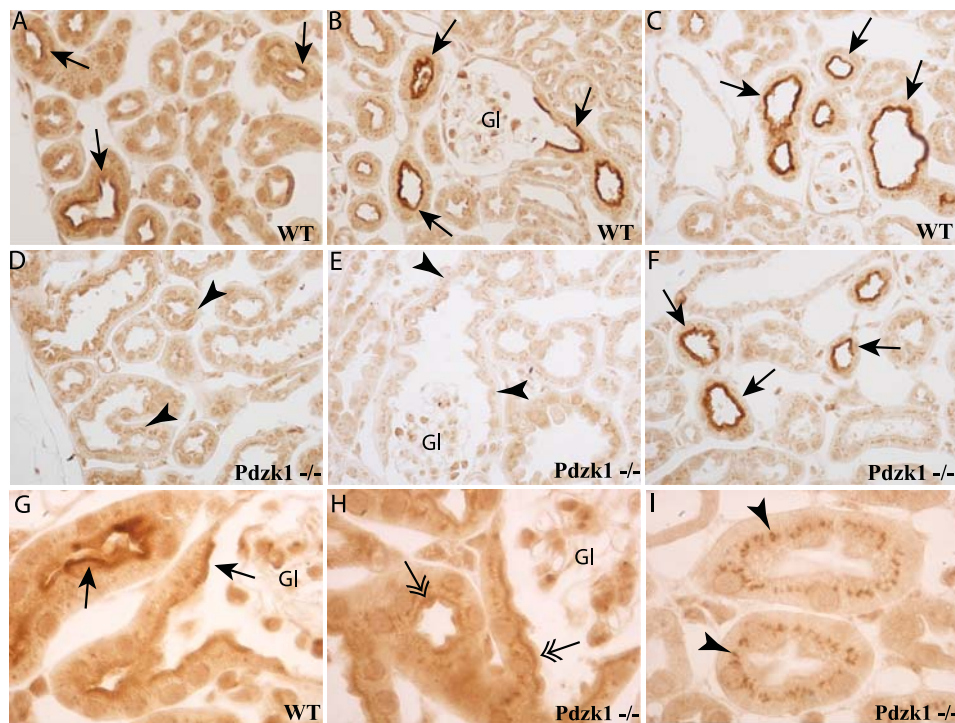


FIGURE 5. NaPi-2c localization by immunohistochemistry showed differential staining pattern in wild type and *Pdzk1*^{-/-} mice. Immunohistochemistry staining also showed differential staining in the cortex region (A and D) with a diminished staining of apical membrane (arrows) from the wild type to the *Pdzk1*^{-/-}. Intracellular staining (arrowheads) was abundantly observed in the *Pdzk1*^{-/-}, but it was not as prominent as with immunofluorescence staining (I). Moreover, a clear continuous line at the base of the brush border or subapical vesicle region (double arrows) was observed in numerous tubules (H). Corticomedullary regions (C and F) showed tubules with stronger signals, but the staining was somewhat reduced in the KO mice. Apical label in the wild type was evident in initial proximal tubule segments (S1) as identified by continuity with Bowman's capsule (B, G, and H). The *Pdzk1*^{-/-} had greatly reduced the apical expression in these segments (E). *Gl*, glomeruli.

ity of proximal tubules had weak NaPi-2c immunolabel in a continuous line at the base of the brush border or subapical vesicle region both in the *Pdzk1*^{-/-} and wild type when analyzed by immunohistochemistry (Fig. 5G). Another noticeable effect is a very strong intracellular staining in the corticomedullary junction and outer medulla of the *Pdzk1*^{-/-} animals, not observed in control animals (Fig. 4). This staining was observed more prominently by immunofluorescence, and it was specific as tested by blocking protection assay with the specific immunogenic peptide (supplemental Fig. S2).

The fact that *Pdzk1*^{-/-} mice only show abnormal regulation in response to chronic low P_i diets in the NaPi-2c transporter, and not in NaPi-2a, suggests that there are different regulatory mechanisms for each of the Na/P_i transporter in the proximal tubule. To exclude a potential role for phosphaturic hormones, we measured the serum levels of PTH and FGF-23. Plasma FGF-23 levels were very similar in the wild type and *Pdzk1*^{-/-} animals with increased levels in mice fed high P_i diets (WT; 1586 ± 180.9 versus 798.5 ± 241.2, *Pdzk1*^{-/-}; 1216 ± 154.1 versus 660.3 ± 123.5 pg FGF-23/ml, high P_i versus low P_i) (Fig.

PDZK1 Regulation of NaPi-2c Transporter

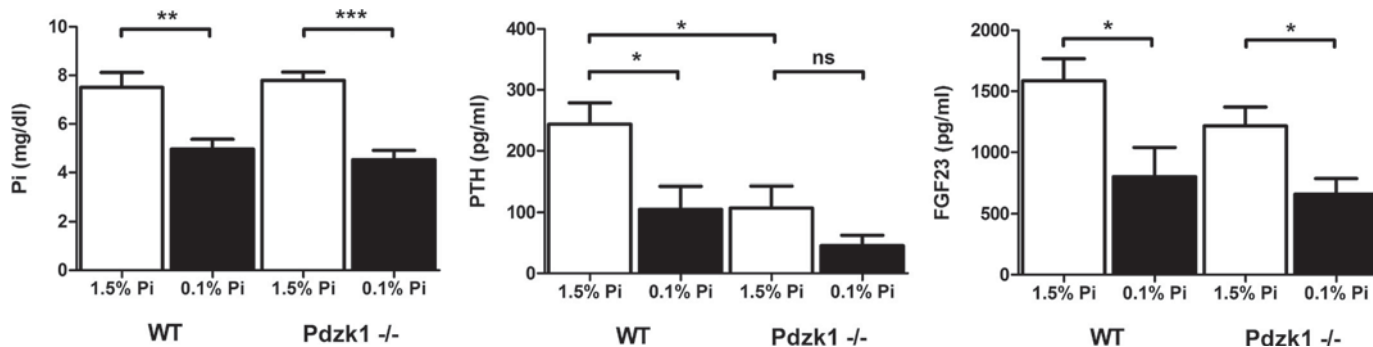


FIGURE 6. Plasma levels of PTH show significant changes between wild type and *Pdzk1*^{-/-} mice. Phosphate, PTH, and FGF-23 hormone levels were quantified in plasma samples of wild type and *Pdzk1*^{-/-} animals fed high and low P_i diets. P_i and FGF-23 did not show significant differences between wild type and KO mice. However, PTH levels were significantly reduced in the KO mice in both dietary conditions. *ns*, not significant.

6C). However, plasma PTH levels showed significant differences between wild type and *Pdzk1*^{-/-} animals (Fig. 6B). *Pdzk1*^{-/-} animals fed high P_i diets have lower PTH levels than wild type animals (WT, 243.7 ± 35.1 versus *Pdzk1*^{-/-}, 107.3 ± 35.8 pg of PTH/ml; *p* = 0.0164). Animals fed low P_i diets showed similar differences, which, however, were not statistically significant (WT, 104.7 ± 38.15 versus *Pdzk1*^{-/-}, 45.48 ± 17.17 pg of PTH/ml; *p* = not significant).

NaPi-2c and NaPi-2a Interactions with PDZK1 and NHERF-1 Measured by FLIM-FRET—The pronounced lack of regulation of NaPi-2c observed in the PDZK1 null mice suggests a more important role of PDZK1 for NaPi-2c than NaPi-2a function. Differences in the affinity or specificity of the interactions with PDZ proteins could explain the opposite effects observed in this KO model. We investigated these differences through the measurement of the proximity of fluorescent protein-labeled Na/P_i transporters and PDZ proteins expressed in living OK cells by FRET.

When FRET occurs (generally if the two fluorophores are within 10 nm), the fluorescence intensity of the acceptor may increase at the expenses of the intensity of the donor. The occurrence of FRET also induces a reduction in the excited state lifetime of the donor. Because the measure of lifetime does not depend in general on the concentration of the fluorophores in the sample, it often provides several advantages with respect to intensity-based methods for the measurement of FRET. Methods for measuring fluorescence lifetime are generally classified as time or frequency domain methods (36). Here we used a digital frequency domain setup, the FLIMBox (27), coupled to a confocal laser scanning microscope, to perform FLIM.

The analysis of lifetime data appears to be complex and somewhat misleading, especially when the decay of the observed species is characterized by the sum of two or more exponentials (as is the case of fluorescent proteins). To address this issue, we analyzed and interpreted FLIM data using the concept of the phasor (28–31). Single-exponential and multi-exponential decays correspond to well defined single phasors, the analysis of which does not require fitting data to exponential components. The FRET process induces a reduction in the lifetime of the donor, and in the phasor space it corresponds to a shifting of the phasor of the donor. Generally, in the case of intermolecular FRET, the observed shift depends on the efficiency of the interaction and the fraction of molecules undergoing FRET.

Previous studies have shown interaction of both NaPi-2a and NaPi-2c with PDZK1 and NHERF-1 by using biochemical techniques (15). Here we used the FLIM-FRET approach to study the putative differential affinity interactions of the Na/P_i transporters.

Figs. 7 and 8 show representative images of OK cells transfected with donor only and with donor plus acceptor species, for different pairs of NaPi-PDZ proteins. The corresponding phasor plot is reported to the right side of the images containing the points associated with the pixels of the two images. Because of noise, experimental data are scattered around the average position of the phasor. In the zoomed region are highlighted the two clusters corresponding to the two cells. The phasor of the cell co-transfected with donor and acceptor species is shifted toward the direction of lower lifetimes showing the occurrence of FRET.

Intensity images and the corresponding phasor plots of transfected cells to study the interactions of the pairs NaPi-2a/PDZK1 and NaPi-2c/PDZK1 are shown in Fig. 7. FRET is observed between NaPi-2a and PDZK1 as shown by the shift of the lifetime when comparing Cer-NaPi-2a (donor) with Cer-NaPi-2a/EYFP-PDZK1 (donor/acceptor) in the phasor plot (Fig. 7, upper row). The pair NaPi-2c/PDZK1 also showed FRET occurrence with a similar shift in the phasor plot (Fig. 7, lower row). The FRET efficiency was quantified for each pair of proteins following the procedure described under “Experimental Procedures.” FRET efficiency of NaPi-2c/PDZK1 (0.41 ± 0.0017) is significantly higher than NaPi-2a/PDZK1 efficiency (0.32 ± 0.0005). However, we have to be cautious when considering that NaPi-2c has a stronger interaction with PDZK1 than NaPi-2a. In this case, the two transporters interact with different PDZ domains of PDZK1, and most likely they will be at different distances, one of the factors that most drastically change FRET efficiency (supplemental Fig. S7). Both transporters showed robust interaction with PDZK1 in accordance with previous studies that used diverse biochemical techniques (12–15).

Because the lack of regulation by low P_i diet of NaPi-2c in the *Pdzk1*^{-/-} mice cannot be explained by differential affinity interactions with PDZK1, we decided to test another PDZ protein. NHERF-1 has been shown to play an important role in the regulation of NaPi-2a (37–40). The interaction of NHERF-1 with both NaPi-2a and NaPi-2c was determined by using different biochemical techniques (12, 13, 15). NHERF-1 has been

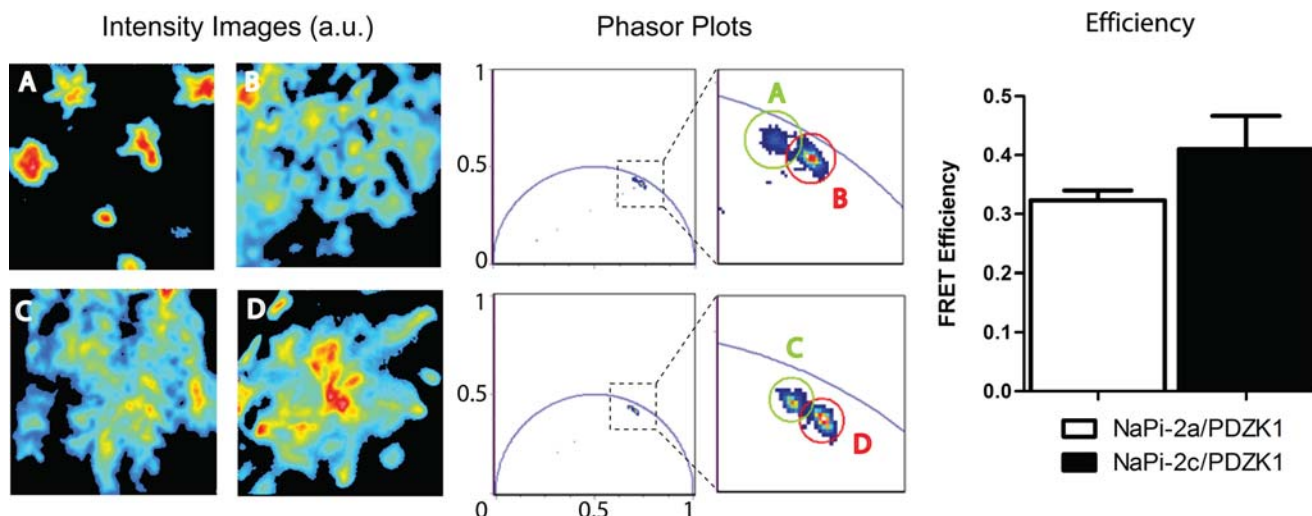


FIGURE 7. FLIM-FRET of Cer-NaPi-2a and Cer-NaPi-2c versus EYFP-PDZK1. Intensity images of cells transfected with Cer-NaPi-2a (A), Cer-NaPi-2a and EYFP-PDZK1 (B), Cer-NaPi-2c (C), and Cer-NaPi-2c and EYFP-PDZK1 (D). The corresponding phasor plots are reported to the right of the images. The phasors of the donor plus acceptor (B and D) are shifted with respect to the donor only (A and C, respectively), indicating the occurrence of FRET. A graphical representation of the FRET efficiency (calculated as explained under “Experimental Procedures” and supplemental Fig. S6) shows a significantly slightly higher value in the case of the pair NaPi-2c/PDZK1.

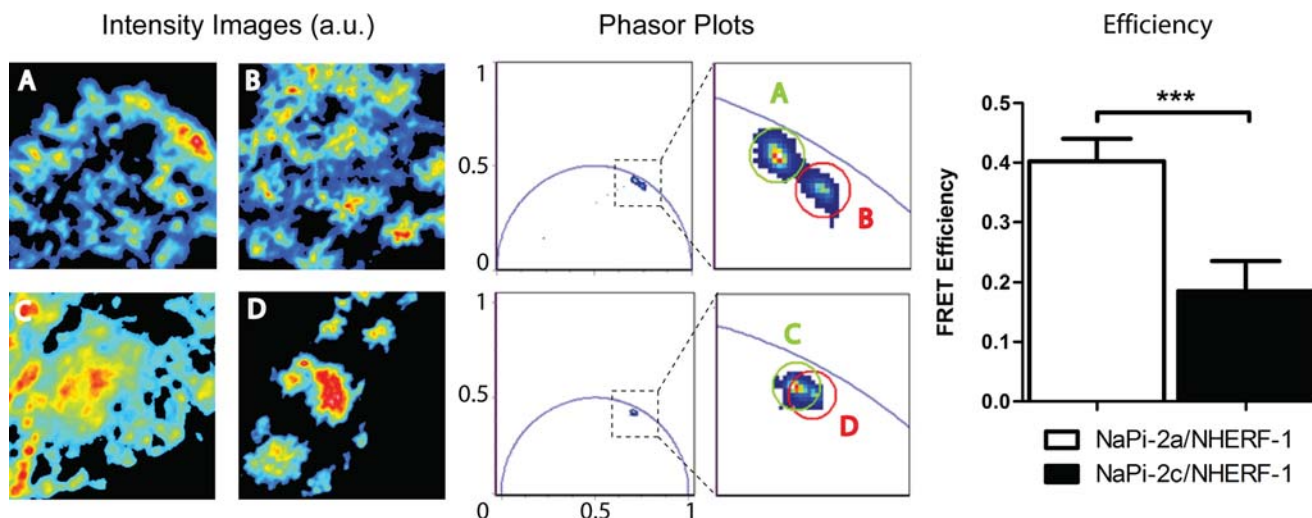


FIGURE 8. FLIM-FRET of Cer-NaPi-2a and Cer-NaPi-2c versus EYFP-NHERF-1. Intensity images of cells transfected with Cer-NaPi-2a (A), Cer-NaPi-2a and EYFP-NHERF-1 (B), Cer-NaPi-2c (C), and Cer-NaPi-2c and EYFP-NHERF-1 (D). The corresponding phasor plots are reported to the right of the images. The phasors of the donor plus acceptor (B and D) are shifted with respect to the donor only (A and C, respectively), indicating the occurrence of FRET. A graphical representation of the FRET efficiency shows a significantly higher value in the case of the pair NaPi-2c/NHERF-1, indicating a lower affinity compared with NaPi-2a.

proposed to act in a compensatory way to prevent the loss of NaPi-2a adaptation in the *Pdzk1*^{-/-} model (20).

In Fig. 8, we analyzed the interaction of the pairs NaPi-2a/NHERF-1 and NaPi-2c/NHERF-1 by FLIM-FRET analysis. The phasor plot corresponding to the pair NaPi-2a/NHERF-1 shows a strong shift of the lifetime when co-expressing Cer-NaPi-2a and EYFP-NHERF-1 corresponding to FRET occurrence (Fig. 8, upper row). However, the interaction between NaPi-2c and NHERF-1 seems much weaker according to the slight displacement of the lifetime in the phasor plot (Fig. 8, lower row). FRET efficiency calculation of these data shows a very significant difference between NaPi-2a/NHERF-1 (0.40 ± 0.038) and NaPi-2c/NHERF-1 (0.18 ± 0.050). These data suggest that NHERF-1 interacts more strongly with NaPi-2a than with NaPi-2c. In this case we can compare the two Na/P_i transporters because they are supposed to interact with the first PDZ

domain of NHERF-1, and therefore they should have similar interacting distance between fluorophores (supplemental Fig. S7).

The efficiency of the FRET process is related to many factors including the particular fluorescent pair used and the relative spatial distribution of the two probes when the two constructs are in the bound state. Another important parameter in intermolecular FRET experiments is the fraction of donors undergoing FRET. Indeed, in the simplest of the cases, donors can be found in either a FRET or no-FRET state, depending on whether the proteins are in a bound or unbound state. The presence of donors in the no-FRET state (unquenched donors) makes the determination of FRET efficiency less straightforward. On the other hand, the fraction of donors in a bound state provides a parameter that can be biologically relevant *per se* when protein interactions are investigated in live cells.

PDZK1 Regulation of NaPi-2c Transporter

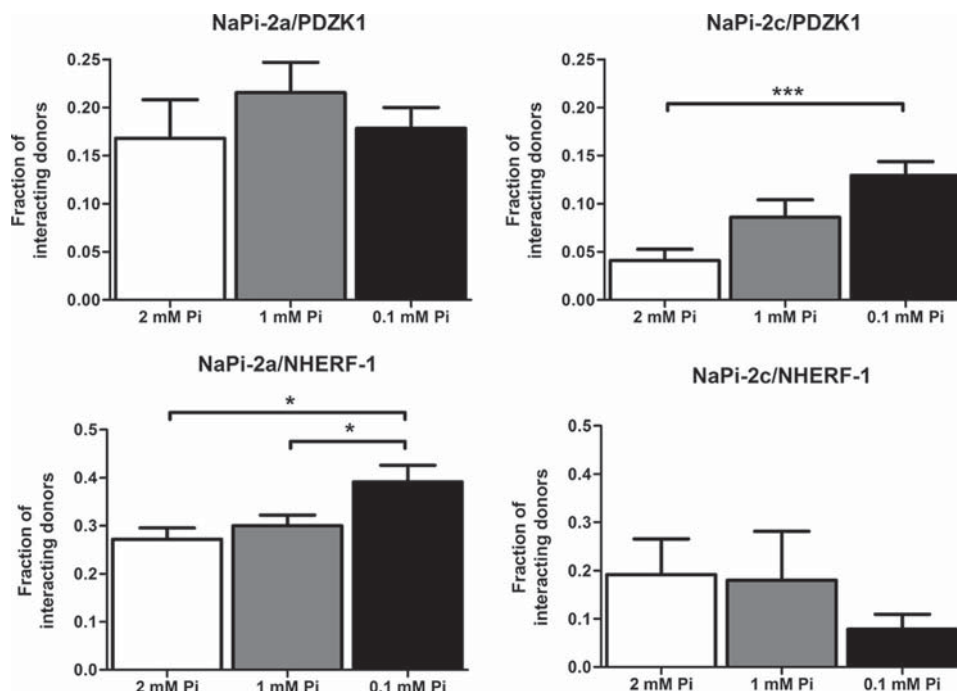


FIGURE 9. Fraction of interacting donors at different P_i content for the different NaPi/PDZ pairs as obtained from the phasor analysis of FRET data. A significant increase of interacting donors was observed for the pair NaPi-2c/PDZK1 at low P_i concentrations (0.1%) in the medium, whereas the pair NaPi-2c/NHERF-1 was not affected. A similar increase of interacting donors was shown for the pair NaPi-2a/NHERF-1 with no changes for NaPi-2a/PDZK1. These results highlight the importance of the interaction NaPi-2c/PDZK1 in the adaptive response to low P_i concentrations.

We followed this approach to study the behavior of the interactions between Na/P_i transporters and PDZ proteins under different P_i concentrations. The FRET efficiency measured from cells adapted to different contents of P_i (2, 1, and 0.1 mM) in the extracellular medium did not change significantly for any of the Na/P_i-PDZ protein pairs under study. Instead, a significant variation was observed in some cases in the fraction of interacting donors. In response to low P_i (0.1 mM) concentrations, a significant increase in the fraction of interacting donors for NaPi-2c/PDZK1 but not for NaPi-2a/PDZK1 was observed (Fig. 9, upper panels). On the other hand, for the interaction with NHERF-1 under low P_i , we observed an opposite behavior with a significant increase in the fraction of interacting donors for NaPi-2a/NHERF-1 but not for NaPi-2c/NHERF-1 (Fig. 9, lower panels).

In our opinion, these findings highlight the importance of the specific interactions NaPi-2a/NHERF-1 and NaPi-2c/PDZK1 during the response to a dietary change of P_i . When cells are adapted to a reduced concentration of P_i , increased fractions of NaPi-2a and NaPi-2c are found in a bound state with NHERF-1 and PDZK1, respectively. These results supporting a more important role for PDZK1 in the adaptation to low P_i of NaPi-2c are in agreement with the results obtained with the *Pdzk1*^{-/-} model. The low affinity interactions showed between NaPi-2c and NHERF-1 would agree also with the lack of compensatory mechanism in the adaptation in the *Pdzk1*^{-/-} model, in contrast to the effects on NaPi-2a.

DISCUSSION

The scaffolding-like PDZ proteins have been involved in the regulation of numerous receptor and transporter proteins (41–46). In the case of the renal Na/P_i transporters, NaPi-2a interact

with and are susceptible to be regulated by several PDZ proteins including the NHERF family members (NHERF-1, 2, 3, and 4) (12–17), Shank2E (19, 47), and CAL (18). The best studied of these proteins until now are the members of the NHERF family, NHERF-1 and PDZK1 (NHERF-3). Although both PDZ proteins have been proved to interact with NaPi-2a and NaPi-2c in *in vitro* assays, a functional relationship with these proteins is still missing. Here we aim to understand the physiological relevance of these interactions using the PDZK1-deficient mice as a model to study the putative differential regulation of the two Na/P_i co-transporters.

Our study showed a significantly impaired up-regulation of NaPi-2c protein levels in the apical membrane of *Pdzk1*^{-/-} mice compared with the wild type animal fed low P_i diets. However, NaPi-2a adaptation to the same conditions was intact. Capuano *et al.* (20) were able to show a slightly decreased expression of NaPi-2a in the *Pdzk1*^{-/-} under high P_i diet; however, we did not see any significant differences. Moreover, we could not find significant differences in urine P_i excretion between wild type and *Pdzk1*^{-/-} animals fed high P_i diets (supplemental Fig. S7), whereas the study by Capuano *et al.* reported an increased phosphaturia in the KO animals. These discrepancies could be due to the fact that we used a higher concentration in the high P_i diets: 1.2% P_i in their study versus 1.5% P_i in ours. The higher dietary P_i could cause minimal NaPi-2a transporter expression and exacerbated phosphaturia in the wild type, and we would miss the reported effects. The deficient adaptation of the NaPi-2c protein levels suggests a more important role for the PDZK1 protein that is not required or can be compensated by other PDZ proteins in the case of the NaPi-2a adaptation. The impaired adaptation of NaPi-2c in the

Pdzk1^{-/-} seems to be independent of transcriptional regulation because higher NaPi-2c mRNA expression does not correlate with the lower apical protein levels observed under low P_i conditions. We consider this effect as an attempt to compensate the deficient apical expression of NaPi-2c in the *Pdzk1*^{-/-} model.

Total membrane renal homogenates in wild type animals fed low P_i diets show an increased expression of both NaPi-2a and NaPi-2c, suggesting an increased rate of *de novo* protein synthesis and/or reduced degradation rate. *Pdzk1*^{-/-} mice show a significantly deficient up-regulation of NaPi-2c also in total membranes and non-BBM fractions. These results were confirmed by immunofluorescence and immunohistochemistry staining of the transporter, showing a clear reduction of NaPi-2c in the apical membrane in the KO mice. In the cortical tubules, NaPi-2c disappeared completely from the microvilli, whereas juxtamedullary tubules still showed apical staining, although clearly reduced *versus* the wild type. It remains to be determined whether this behavior implies differences in the regulation of NaPi-2c between cortical and juxtamedullary tubules. Subapical staining of NaPi-2c was prominently observed in the *Pdzk1*^{-/-} animal. This kind of subcellular location has been observed 4 h after switching to a high P_i diet when NaPi-2c is translocated from the microvilli to a subapical region (10). This finding suggest that in the *Pdzk1*^{-/-} mice, NaPi-2c is able to traffic to the membrane, but it cannot be efficiently retained in the microvilli.

Based on the preliminary electrolyte analysis of the *Pdzk1*^{-/-} *versus* wild type animal (22), Capuano *et al.* (20) proposed that it was very unlikely that PDZK1 deficiency would cause changes in the levels of the phosphaturic hormones. Indeed, the results of our analysis show that the blunted regulation of NaPi-2c is not induced by phosphaturic hormonal changes. However, PTH levels were reduced in *Pdzk1*^{-/-} animals, although these differences are unlikely to be related to the reduced adaptation of NaPi-2c because increased PTH signaling in fact induces endocytosis and decreased BBM expression of both Na/P_i transporters. It would be more plausible to think that decreased PTH levels, which would promote brush border localization of both NaPi-2c and NaPi-2a, are trying to compensate for the reduced stability of NaPi-2c and probably NaPi-2a in the brush border. Plasma P_i levels were higher in animals under high P_i diets without differences between wild type and *Pdzk1*^{-/-} animals as reported before (20, 22).

However, the most intriguing question presented by this study is why NaPi-2a is able to fully adapt to low P_i conditions in the absence of PDZK1, whereas NaPi-2c is not. Compensatory mechanisms mediated presumably by NHERF-1 have been suggested to explain that *Pdzk1*^{-/-} is able to adapt NaPi-2a under chronic and acute dietary changes (20). However, the discrepancies between NaPi-2a and NaPi-2c were not expected, because both Na/P_i transporters have been shown to interact with PDZK1 and NHERF-1 (15). Study of the interactions between Na/P_i transporters and PDZK1 and NHERF-1 by using the FLIM-FRET technique resulted in differential FRET efficiency between both transporters. Although for PDZK1 interactions both NaPi-2a and 2c showed strong FRET occurrence, the interactions with NHERF-1 showed a much stronger inter-

action for NaPi-2a. It is important to be careful interpreting the results from FRET measurements because factors such as the distance between both fluorophores can influence greatly the values of efficiency. Because this distance is specific for each pair of proteins, it is not always suitable to compare affinities of interaction between different pairs. In our case of study, we could compare FRET efficiency interactions of the pairs NaPi-2a/NHERF-1 and NaPi-2c/NHERF-1 because both transporters have presumably a similar structure, and both interact with the first PDZ domain of NHERF-1. However, NaPi-2a interacts with the PDZ3 of PDZK1, whereas NaPi-2c interacts with PDZ2, suggesting greater differences in the distances between the fluorophores even without knowing exactly the folding structure of PDZK1 (supplemental Fig. S8). Our results imply differences in the affinity interaction of NHERF-1 with NaPi-2a and 2c that could explain why NaPi-2c is not able to adapt to low P_i diets in the *Pdzk1*^{-/-}. The previous study that identified these interactions suggested already that the interaction NaPi-2c/NHERF-1 differs in nature from the interaction NaPi-2c/PDZK1. These results were supported by the finding that under lower concentrations of P_i in the medium, the number of interacting proteins was increased for the pair NaPi-2c/PDZK1 but not for NaPi-2c/NHERF-1 pair.

Our results suggest that PDZK1 plays a role in the stabilization/retention of NaPi-2c in the microvilli more than in the trafficking of the transporter to the apical membrane. Previous studies have suggested a similar role for PDZK1 in the stabilization of NaPi-2a, whereas NHERF-1 could be more involved in the trafficking or insertion on the membrane (20).

In summary, *Pdzk1*^{-/-} mice showed an impaired adaptation of NaPi-2c to chronic low P_i diets that differs from the behavior of NaPi-2a. That impaired adaptation is characterized by reduced apical and total NaPi-2c protein expression and by increased intracellular staining in the *Pdzk1*^{-/-} model. Analysis by FLIM-FRET showed that the interaction between NaPi-2a/NHERF-1 is much stronger than the pair NaPi-2c/NHERF-1. We suggest that NaPi-2c under physiological conditions has to compete with other proteins that interact with greater affinity with NHERF-1, reducing its chances of interaction. This fact would be an important difference in the regulation of NaPi-2a and NaPi-2c, and it would explain the lack of compensatory effect for NaPi-2c in the *Pdzk1*^{-/-}. PDZK1 protein plays an important role in the adaptation of NaPi-2c to low P_i conditions.

Acknowledgment—We thank Dr. David Silver for the generous gift of supplying the anti-PDZK1 antibody and for making the *Pdzk1*^{-/-} mouse model commercially available.

REFERENCES

1. Beck, L., Karaplis, A. C., Amizuka, N., Hewson, A. S., Ozawa, H., and Tenenhouse, H. S. (1998) *Proc. Natl. Acad. Sci. U.S.A.* **95**, 5372–5377
2. Hoag, H. M., Martel, J., Gauthier, C., and Tenenhouse, H. S. (1999) *J. Clin. Invest.* **104**, 679–686
3. Murer, H., Forster, I., and Biber, J. (2004) *Pflugers Arch.* **447**, 763–767
4. Segawa, H., Kaneko, I., Takahashi, A., Kuwahata, M., Ito, M., Ohkido, I., Tatsumi, S., and Miyamoto, K. (2002) *J. Biol. Chem.* **277**, 19665–19672
5. Levi, M., Kempson, S. A., Löttscher, M., Biber, J., and Murer, H. (1996) *J.*

PDZK1 Regulation of NaPi-2c Transporter

- Membr. Biol.* **154**, 1–9
- Miyamoto, K., Ito, M., Tatsumi, S., Kuwahata, M., and Segawa, H. (2007) *Am. J. Nephrol.* **27**, 503–515
 - Forster, I. C., Köhler, K., Biber, J., and Murer, H. (2002) *Prog. Biophys. Mol. Biol.* **80**, 69–108
 - Lötscher, M., Kaissling, B., Biber, J., Murer, H., and Levi, M. (1997) *J. Clin. Invest.* **99**, 1302–1312
 - Levi, M., Lötscher, M., Sorribas, V., Custer, M., Arar, M., Kaissling, B., Murer, H., and Biber, J. (1994) *Am. J. Physiol.* **267**, F900–F908
 - Segawa, H., Yamanaka, S., Ito, M., Kuwahata, M., Shono, M., Yamamoto, T., and Miyamoto, K. (2005) *Am. J. Physiol. Renal Physiol.* **288**, F587–F596
 - Segawa, H., Yamanaka, S., Onitsuka, A., Tomoe, Y., Kuwahata, M., Ito, M., Taketani, Y., and Miyamoto, K. (2007) *Am. J. Physiol. Renal Physiol.* **292**, F395–F403
 - Gisler, S. M., Stagljar, I., Traebert, M., Bacic, D., Biber, J., and Murer, H. (2001) *J. Biol. Chem.* **276**, 9206–9213
 - Hernando, N., Déliot, N., Gisler, S. M., Lederer, E., Weinman, E. J., Biber, J., and Murer, H. (2002) *Proc. Natl. Acad. Sci. U.S.A.* **99**, 11957–11962
 - Gisler, S. M., Pribanic, S., Bacic, D., Forrer, P., Gantenbein, A., Sabourin, L. A., Tsuji, A., Zhao, Z. S., Manser, E., Biber, J., and Murer, H. (2003) *Kidney Int.* **64**, 1733–1745
 - Villa-Bellosta, R., Barac-Nieto, M., Breusegem, S. Y., Barry, N. P., Levi, M., and Sorribas, V. (2008) *Kidney Int.* **73**, 456–464
 - Hernando, N., Gisler, S. M., Pribanic, S., Déliot, N., Capuano, P., Wagner, C. A., Moe, O. W., Biber, J., and Murer, H. (2005) *J. Physiol.* **567**, 21–26
 - Wade, J. B., Liu, J., Coleman, R. A., Cunningham, R., Steplock, D. A., Lee-Kwon, W., Pallone, T. L., Shenolikar, S., and Weinman, E. J. (2003) *Am. J. Physiol.* **285**, C1494–C1503
 - Lanaspa, M. A., Giral, H., Breusegem, S. Y., Halaihel, N., Baile, G., Catalán, J., Carrodeguas, J. A., Barry, N. P., Levi, M., and Sorribas, V. (2007) *Am. J. Physiol. Renal Physiol.* **292**, F230–F242
 - McWilliams, R. R., Breusegem, S. Y., Brodsky, K. F., Kim, E., Levi, M., and Doctor, R. B. (2005) *Am. J. Physiol.* **289**, C1042–C1051
 - Capuano, P., Bacic, D., Stange, G., Hernando, N., Kaissling, B., Pal, R., Kocher, O., Biber, J., Wagner, C. A., and Murer, H. (2005) *Pflugers Arch.* **449**, 392–402
 - Lan, D., and Silver, D. L. (2005) *J. Biol. Chem.* **280**, 23390–23396
 - Kocher, O., Pal, R., Roberts, M., Cirovic, C., and Gilchrist, A. (2003) *Mol. Cell Biol.* **23**, 1175–1180
 - Breusegem, S. Y., Takahashi, H., Giral-Arnal, H., Wang, X., Jiang, T., Verlander, J. W., Wilson, P., Miyazaki-Anzai, S., Sutherland, E., Caldas, Y., Blaine, J. T., Segawa, H., Miyamoto, K., Barry, N. P., and Levi, M. (2009) *Am. J. Physiol. Renal Physiol.* **297**, F350–F361
 - Cole, J. A., Forte, L. R., Krause, W. J., and Thorne, P. K. (1989) *Am. J. Physiol.* **256**, F672–F679
 - Blaine, J., Okamura, K., Giral, H., Breusegem, S., Caldas, Y., Millard, A., Barry, N., and Levi, M. (2009) *Am. J. Physiol. Cell Physiol.* **297**, C1339–C1346
 - Breusegem, S. Y., Halaihel, N., Inoue, M., Zajicek, H., Lederer, E., Barry, N. P., Sorribas, V., and Levi, M. (2005) *Am. J. Physiol. Renal Physiol.* **289**, F154–F165
 - Colyer, R. A., Lee, C., and Gratton, E. (2008) *Microsc. Res. Tech.* **71**, 201–213
 - Redford, G. I., and Clegg, R. M. (2005) *J. Fluoresc.* **15**, 805–815
 - Gratton, E., Jameson, D. M., and Hall, R. D. (1984) *Annu. Rev. Biophys. Bioeng.* **13**, 105–124
 - Digman, M. A., Caiolfa, V. R., Zamai, M., and Gratton, E. (2008) *Biophys. J.* **94**, L14–16
 - Clayton, A. H., Hanley, Q. S., and Verveer, P. J. (2004) *J. Microsc.* **213**, 1–5
 - Verveer, P. J., Wouters, F. S., Reynolds, A. R., and Bastiaens, P. I. (2000) *Science* **290**, 1567–1570
 - Caiolfa, V. R., Zamai, M., Malengo, G., Andolfo, A., Madsen, C. D., Sutín, J., Digman, M. A., Gratton, E., Blasi, F., and Sidenius, N. (2007) *J. Cell Biol.* **179**, 1067–1082
 - Rizzo, M. A., Springer, G. H., Granada, B., and Piston, D. W. (2004) *Nat. Biotechnol.* **22**, 445–449
 - Truong, K., and Ikura, M. (2001) *Curr. Opin. Struct. Biol.* **11**, 573–578
 - Suhling, K., French, P. M., and Phillips, D. (2005) *Photochem. Photobiol. Sci.* **4**, 13–22
 - Shenolikar, S., Voltz, J. W., Minkoff, C. M., Wade, J. B., and Weinman, E. J. (2002) *Proc. Natl. Acad. Sci. U.S.A.* **99**, 11470–11475
 - Cunningham, R., E, X., Steplock, D., Shenolikar, S., and Weinman, E. J. (2005) *Am. J. Physiol. Renal Physiol.* **289**, F933–F938
 - Weinman, E. J., Boddeti, A., Cunningham, R., Akom, M., Wang, F., Wang, Y., Liu, J., Steplock, D., Shenolikar, S., and Wade, J. B. (2003) *Am. J. Physiol. Renal Physiol.* **285**, F1225–F1232
 - Cunningham, R., Steplock, D., E, X., Biswas, R. S., Wang, F., Shenolikar, S., and Weinman, E. J. (2006) *Am. J. Physiol. Renal Physiol.* **291**, F896–F901
 - Seidler, U., Singh, A., Chen, M., Cinar, A., Bachmann, O., Zheng, W., Wang, J., Yeruva, S., and Riederer, B. (2009) *Exp. Physiol.* **94**, 175–179
 - Weinman, E. J., Hall, R. A., Friedman, P. A., Liu-Chen, L. Y., and Shenolikar, S. (2006) *Annu. Rev. Physiol.* **68**, 491–505
 - Kato, Y., Watanabe, C., and Tsuji, A. (2006) *Eur. J. Pharm. Sci.* **27**, 487–500
 - Yesilaltay, A., Kocher, O., Rigotti, A., and Krieger, M. (2005) *Curr. Opin. Lipidol.* **16**, 147–152
 - Weinman, E. J., Cunningham, R., and Shenolikar, S. (2005) *Pflugers Arch.* **450**, 137–144
 - Shenolikar, S., Voltz, J. W., Cunningham, R., and Weinman, E. J. (2004) *Physiology* **19**, 362–369
 - Dobrinskikh, E., Giral, H., Caldas, Y. A., Levi, M., and Doctor, R. B. (2010) *Am. J. Physiol.* **299**, C1324–C1334

Supplementary figures

Supplementary figure 1. Expression of PDZK1 protein was totally abolished in renal tissue of the *Pdzk1* *-/-* mouse. Both brush border membrane vesicles (BBMV) and total homogenates were tested with a polyclonal rabbit anti-PDZK1, kindly provided by David Silver, by western blot analysis.

Supplementary figure 2. Specificity of NaPi-2c polyclonal rabbit antibody was tested by peptide blocking assay. A) Western blot analysis of renal BBMV of wild type mice fed high Pi (H Pi) or low Pi (L Pi) diets with anti-NaPi-2c (left; Ab) and with anti-NaPi-2c incubate with its antigenic peptide (right; Ab + peptide). B) Immunofluorescence of *Pdzk1* *-/-* kidney slices stained with anti-NaPi-2c (upper row), anti-NaPi-2c + peptide (middle row) and the same slice with digital increase of the NaPi-2c signal (red) intensity (lower row). Simultaneously actin was stained with phalloidin Alexa-488 (Green). A zoomed image of the merge staining is showed at the side for comparison. Both the apical and the intracellular staining obtained with the NaPi-2c antibody were prevented by using the antigenic peptide.

Supplementary figure 3. BBMV protein expression in male wild type (WT) and *Pdzk1* *-/-* mice in response to chronic adaptation to high (1.5%) and low (0.1%) Pi diets. A similar adaptive response was observed in male *Pdzk1* *-/-* animals with normal adaptation to low Pi diets of NaPi-2a expression in BBM and impaired upregulation of NaPi-2c in *Pdzk1* *-/-* model under the same conditions.

Supplementary figure 4. NaPi-2c shows diminished apical expression in *Pdzk1* *-/-* mice. Renal section derived from wild type and *Pdzk1* *-/-* mice were stained for actin (with phalloidin, green), NaPi-2c (red) and nuclei (blue). NaPi-2c staining in the superficial cortex (SC) tubules (first row) is clearly weaker than in juxtamedullary tubules (third row) in the wild type. NaPi-2c apical membrane expression is totally blunted in SC tubules of *Pdzk1* *-/-* resulting in an increased intracellular perinuclear staining (second row). JM tubules of *Pdzk1* *-/-* showed a diminished apical expression with increased subapical staining but still conserved partial NaPi-2c expression in the apical membrane (fourth row).

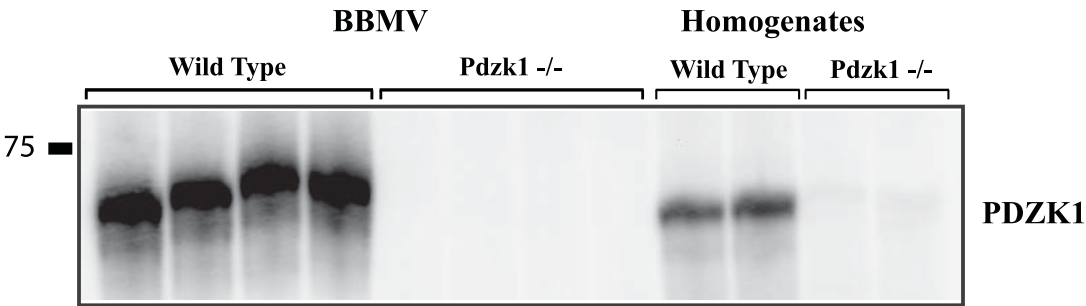
Supplementary figure 5. Analysis of FRET data in the phasor plot. Given the phasors of the unquenched donor (D_{unq}) and of the autofluorescence (af), the phasor of the quenched donor (D_q) is expected to lie along a calculated trajectory of variable efficiency (black solid line). The phasor of a mixture of quenched and unquenched donors is a linear combination of the phasors of D_q and D_{unq} and will lie along the segment connecting them (dashed line), at a distance from D_{unq} proportional to the fraction of interacting donors (f_q).

Supplementary figure 6. Procedure to calculate the FRET efficiency and the fraction of interacting donors. The phasor coordinates associated with the Donor only (D only) and Donor plus Acceptor samples (D+A) are fitted to a linear trend. The intersection between the trend line and the calculated trajectory of variable efficiency yields the extrapolated phasor of the Donor quenched with efficiency E. The fraction of quenched and unquenched donors in the Donor plus Acceptor samples is then calculated. Experiment sample: Cerulean-NaPi-2a vs EYFP-NHERF-1.

Supplementary figure 7. Phosphate excretion measurements. Urine levels of phosphate and creatinine were measured in wild type and *Pdzk1* *-/-* animals fed high and low Pi diets during one week. Data was plotted as Urine Pi/Urine Creatinine ratio and Fractional Excretion Index (FEI) of Pi defined previously as $\text{Urine Pi}/(\text{Urine Creatinine} \times \text{Plasma Pi})$. Both measured parameters did not show any significant differences between wild type (WT) and *Pdzk1* *-/-* animals. An extensive increase in phosphaturia was observed in the animals fed a high Pi diet in both groups.

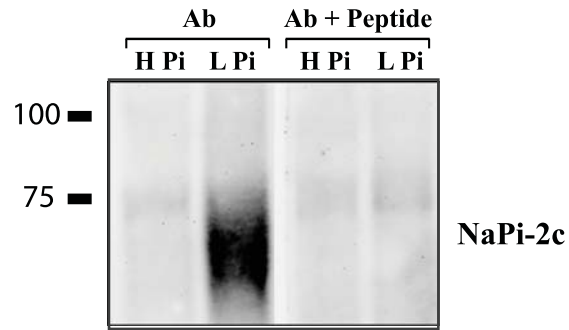
Supplementary figure 8. Schematic representation of the molecular interactions between the Na/Pi transporters and the PDZ proteins PDZK1 and NHERF-1. The Na/Pi transporters are represented as transmembrane proteins (NaPi-2c-green; NaPi-2a-yellow) fused to the Cerulean fluorescent protein (Blue) and PDZK1 (with 4 different PDZ domains) and NHERF-1 (with 2 PDZ domains and the ERM-binding motif in the C-terminus) fused to EYFP (Green). NaPi-2c interacts with the second while NaPi-2a interacts with the third domain of PDZK1 suggesting that the distance between the fluorescent proteins (FPs) will be larger for the interaction NaPi-2a/PDZK1. In the other hand, both NaPi-2c and NaPi-2a have been proved to interact with the first PDZ domain of NHERF-1 and presumably the distance between the FPs should be in the same range. The relative distances showed below have been calculated considering: FP length - 4 nm, PDZ domain length- 3.5 nm and interdomain aminoacid chain being in alpha-helix structure- 0.15nm/residue. It is important to notice that these distances are referring to the totally extended protein conformation and that under physiological conditions the multiprotein complex could be folded in a more compact structure.

Supplementary Figure 1

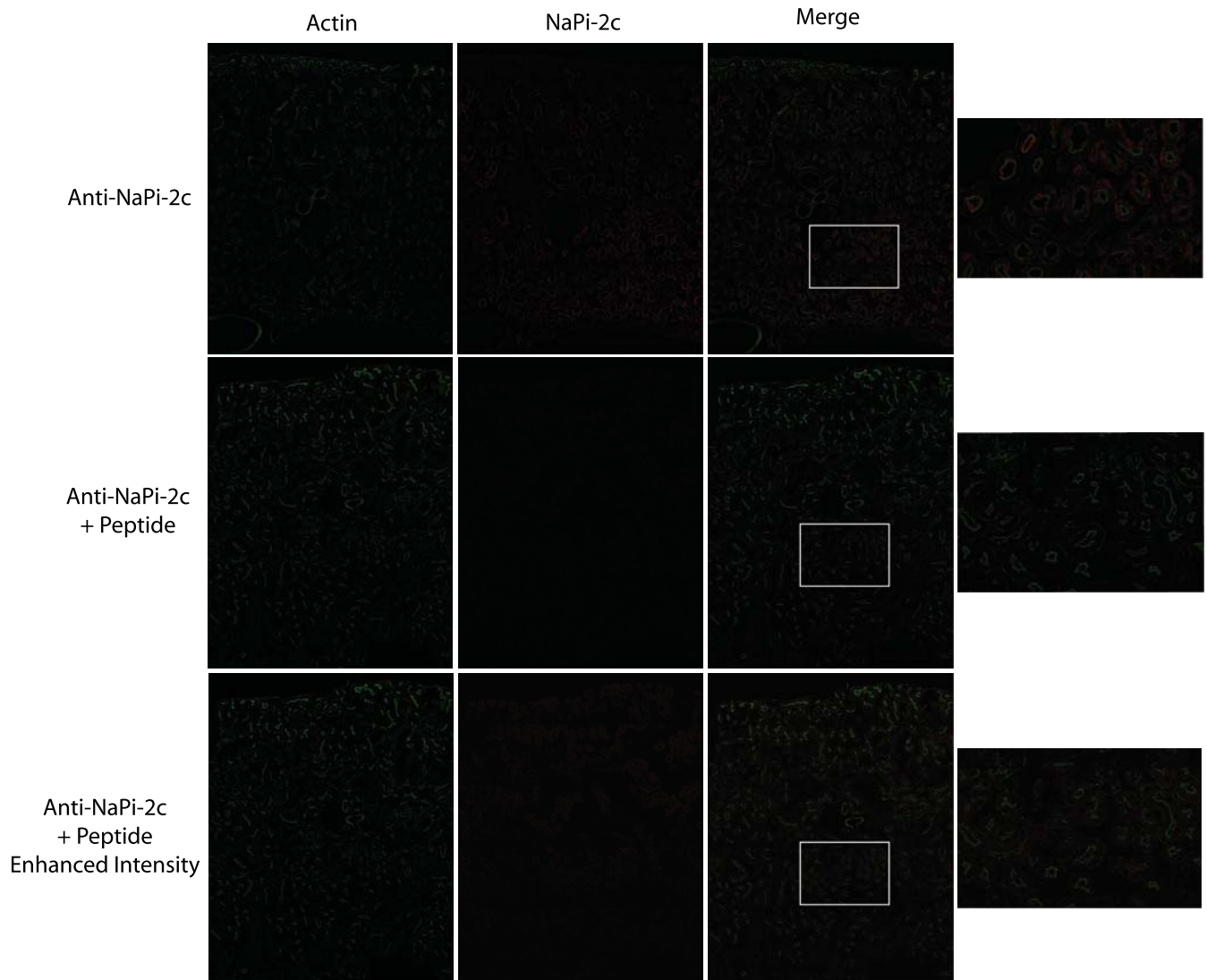


Supplementary Figure 2

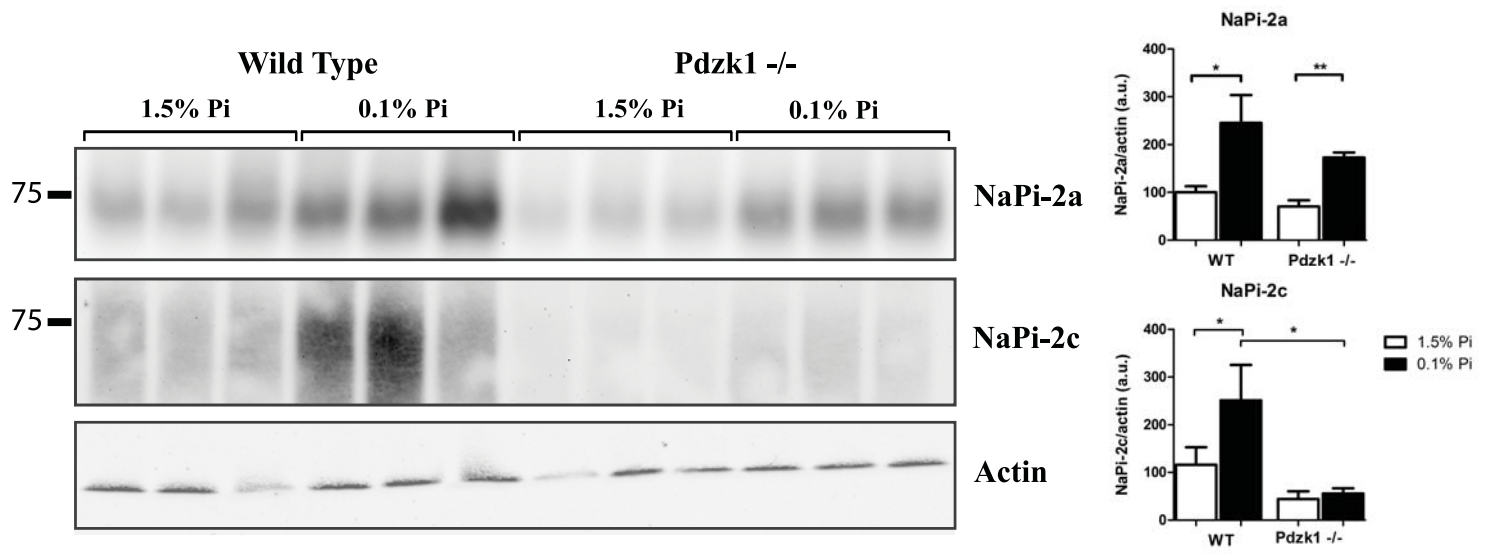
A



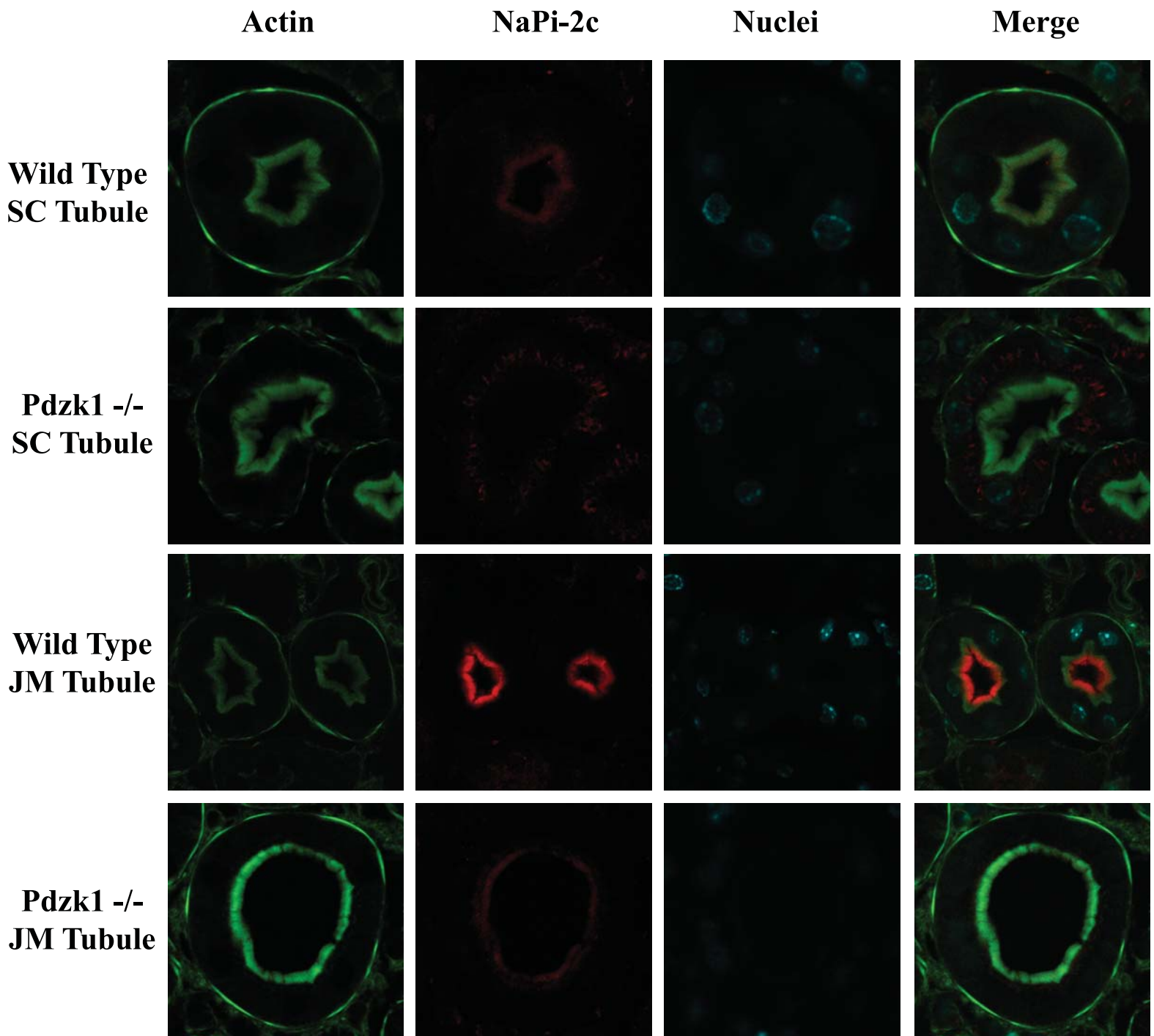
B



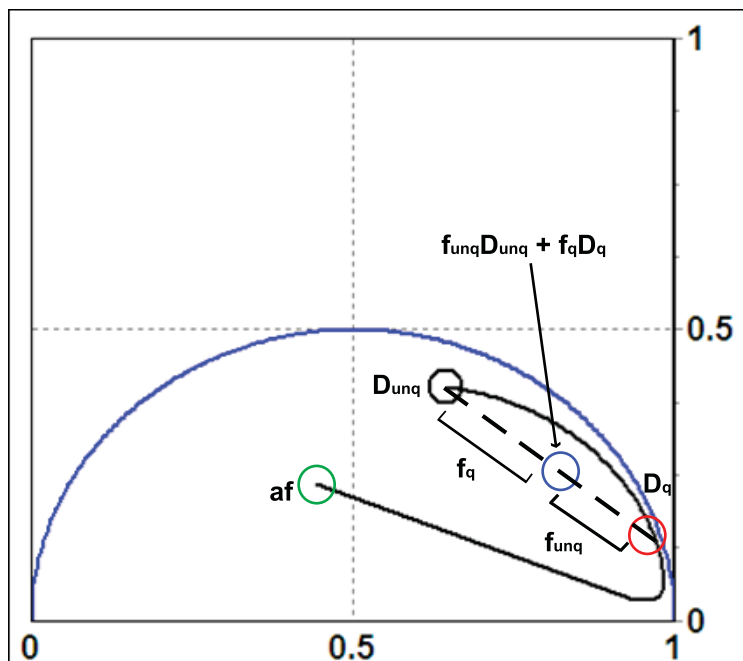
Supplementary Figure 3



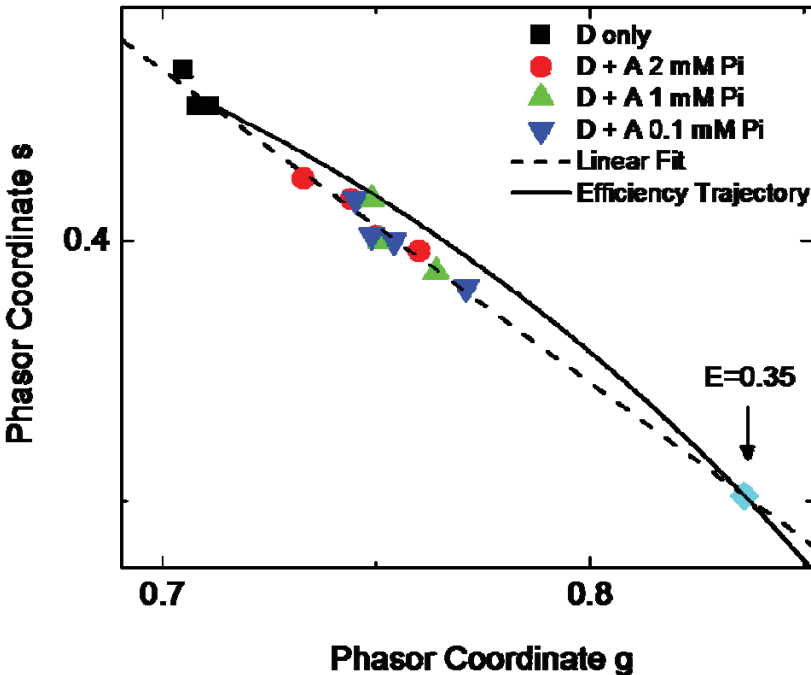
Supplementary Figure 4



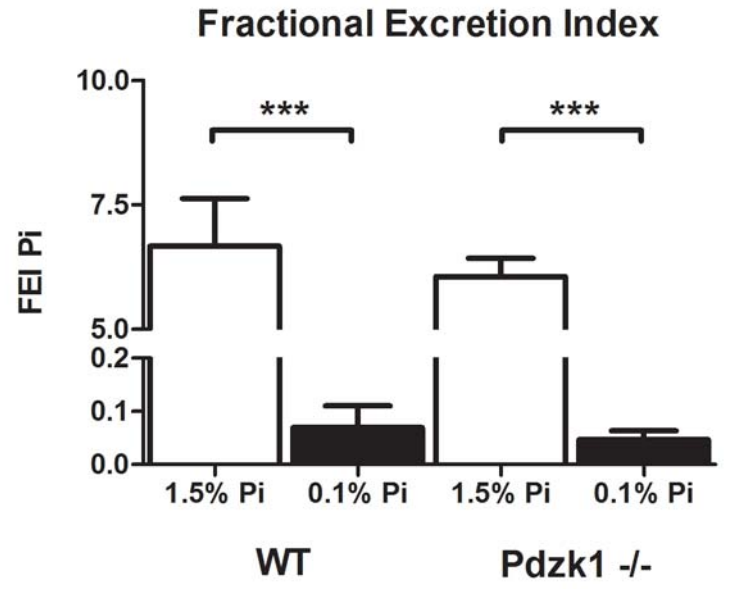
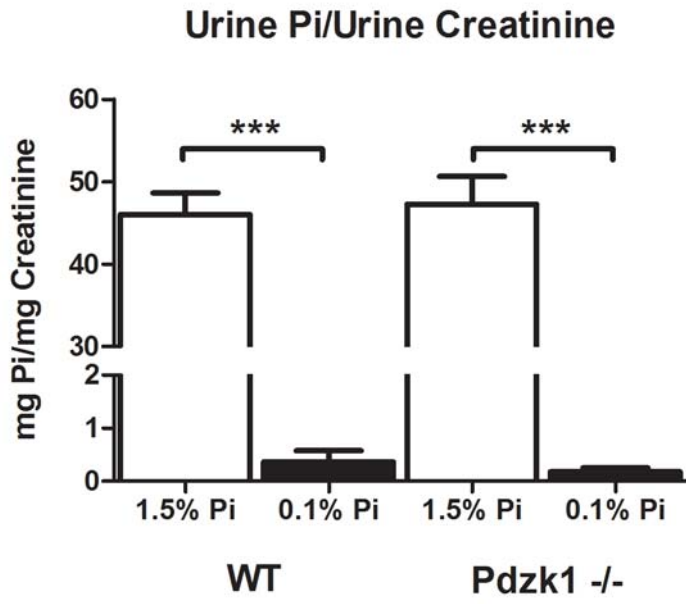
Supplementary Figure 5



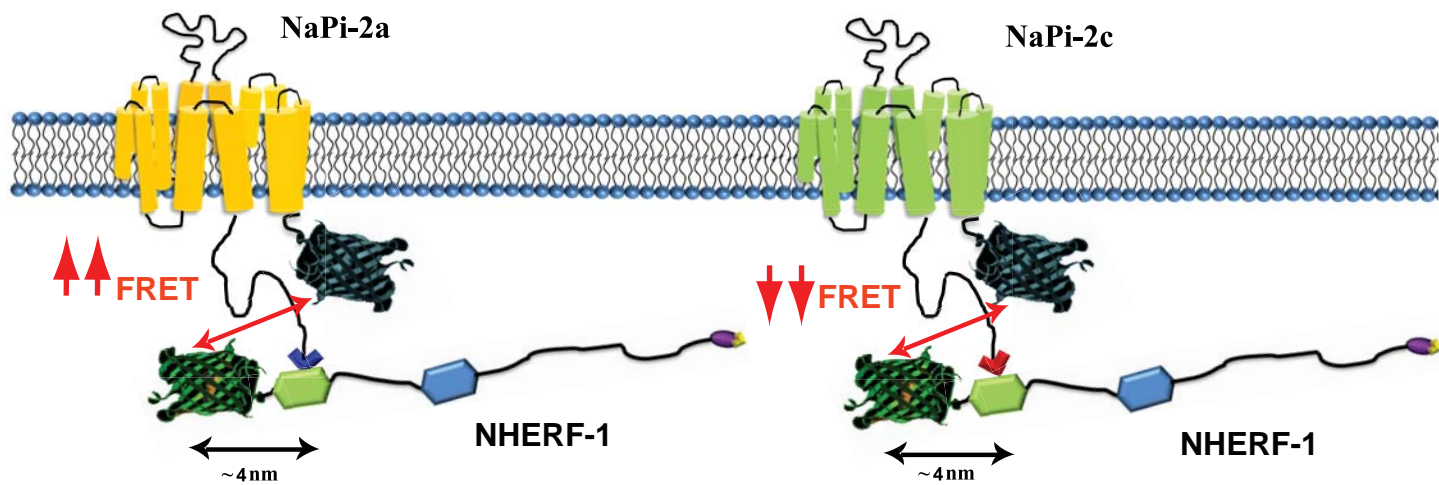
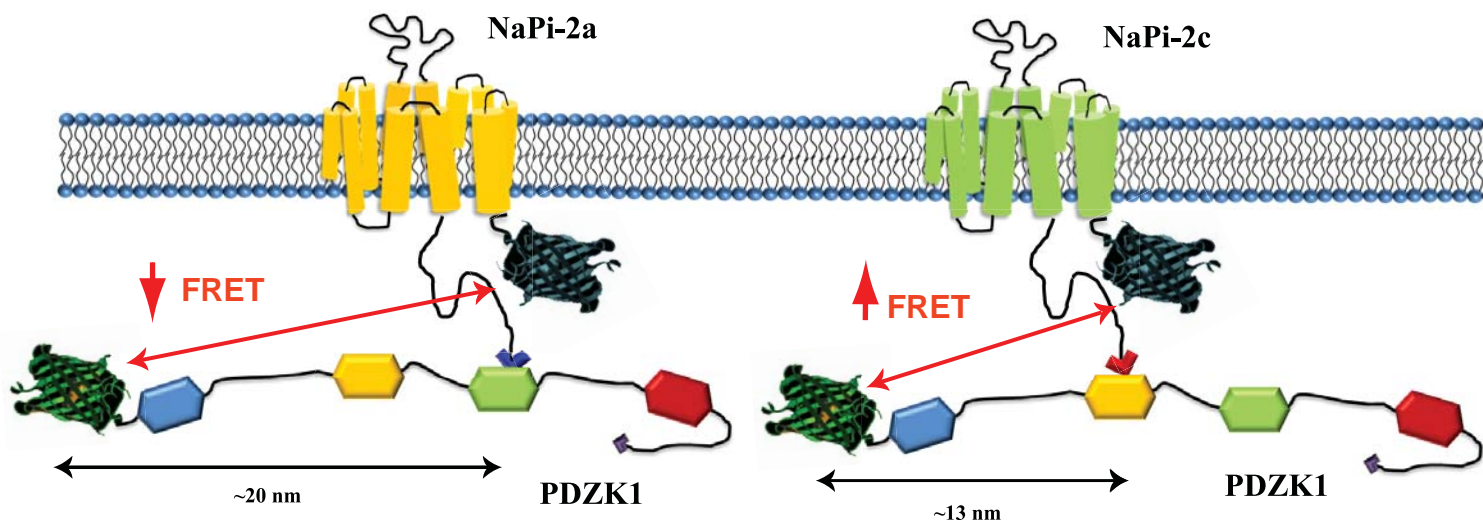
Supplementary figure 6.








Supplementary Figure 7



Supplementary Figure 8



Legend

-  Green Fluorescent protein
-  Cerulean Fluorescent protein
-  PDZ domain
-  PDZ binding motif
-  ERM binding domain